Supporting Information

The Reaction Electronic Flux Perspective on the Mechanism of the Zimmerman Di-π-Methane Rearrangement

Ricardo A. Matute*,[1,2,3] Patricia Pérez,[4] Eduardo Chamorro,[4] Nery Villegas-Escobar,[1] Diego Cortés-Arriagada,[5] Bárbara Herrera,[1] Soledad Gutiérrez-Oliva,[1] and Alejandro Toro-Labbé*,[1]

[1] Laboratorio de Química Teórica Computacional (QTC), Facultad de Química, Pontificia Universidad Católica de Chile, Casilla 306, Correo 22, Santiago, Chile

[2] Division of Chemistry and Chemical Engineering, California Institute of Technology, Pasadena, CA 91125

[3] Centro Integrativo de Biología y Química Aplicada (CIBQA), Universidad Bernardo O Higgins, Santiago 8370854, Chile

[4] Universidad Andres Bello, Facultad de Ciencias Exactas, Departamento de Ciencias Químicas, Avenida República 275, 8370146 Santiago, Chile

[5] Programa Institucional de Fomento a la Investigación, Desarrollo e Innovación, Universidad Tecnológica Metropolitana, Ignacio Valdivieso 2409, P.O. Box 8940577, San Joaquín, Santiago, Chile)

Corresponding Authors

*E-mail (R.A.M.): rmatute@caltech.edu

*E-mail (A.T.L.): atola@uc.cl

TABLE OF CONTENTS

1. Theoretical Background for Reaction Force Model

Reaction Force:

To characterize reaction mechanisms, it is first necessary to follow the reaction along a reaction coordinate and monitor the sistem's properties at each point along it. The most important property is the energy, wich gives information about the reaction energy (ΔE^o) and the height of the reaction barrier ($\Delta E^{\neq}$), getting the thermodynamics and the kinetics of the reaction with a few transformations.

When deriving the reaction energy, leads to the Hellman-Feynman reaction force, and it is a global property that helps to get helpful information about the chemical events that are taking place in any given reaction.[1-6]

$$F(\xi) = -\left(\frac{dE}{d\xi}\right) \tag{1}$$

In a single step potential, this index presents two critical points, a minimum ξ_1 that defines the reactant zone, (from ξ_R to ξ_1), where the structural rearrangements occur, and the maximum of the reaction force, ξ_2. Where from is ξ_2 to this point is defined the transition state zone, were all the electronic rearrangements take place, and from ξ_2 to ξ_P is defined the product zone. were structural relaxation of the system occurs in order to give products. Note that this partition of the reaction coordinate defines reaction works, that can be associated to structural and electronic rearrangements, such as:

$$W_1 = -\int_P^{\xi_1} F(\xi)d\xi > 0 \qquad W_2 = -\int_{\xi_1}^{TS} F(\xi)d\xi > 0$$
$$W_3 = -\int_{TS}^{\xi_2} F(\xi)d\xi < 0 \qquad W_4 = -\int_{\xi_2}^{P} F(\xi)d\xi < 0 \tag{2}$$

W_1 corresponds to the structural activation, W_2 measures the energy to electronic activation to reach the transition state. After the transition state zone, the structural relaxation is associated to W_3 and the electronic work tp reach the product is W_4.[1-6] Since W_1 and W_4 are defined as structural works, and W_2 and W_3 are defined as electronic works, it is possible to quantify the energy and the barrier of the system in terms of this two contributions. $\Delta E^o = W_1+W_2+W_3+W_4$ and $\Delta E^{\neq} = W_1+W_2$.

2. Theoretical Background for Reaction Electron Flux

Electronic Chemical Potential:

Into conceptual DFT there are defined various response functions, which correspond to the chemical reactivity of a system, also known as global and local descriptors.[7,8] One of the most important properties is the electronic chemical potential, or the escaping tendency of electrons from an equilibrium system, and associated to the negative of electronegativity defined by Mulliken. For an N electron system, chemical potential is defined as:[7,8]

$$\mu = \left(\frac{\partial E}{\partial N}\right)_{v(\vec{r})} = -\chi \tag{2}$$

Owing to the discontinuity of the energy along the number of electrons, this index can be quantified using the finite difference approximation to values of the ionization energies (I) and the electron affinities (A) and with the Koopmans theorem to the energies of frontier orbitals HOMO and LUMO molecular orbitals ε_{HOMO} and ε_{LUMO}.[7,8]

$$\mu \approx -\frac{I+A}{2} \approx \frac{\varepsilon_{LUMO}+\varepsilon_{HOMO}}{2} \tag{3}$$

Reaction Electronic Flux.

The relation between electron flux and the gradient of the chemical potential is used to define the reaction electronic flux (REF).[5,9-12] The reaction electronic flux indicates the electronic reorganization in a chemical reaction and is defined as:

$$J(\xi) = -\left(\frac{d\mu}{d\xi}\right) \tag{4}$$

In analogy to thermodynamics, this property can be associated to the spontaneity of the electronic processes. When J(ξ) is positive, is associated to spontaneous reorganization of the electron cloud, indicating bond forming or strengthening, when the values are negative, the change will be nonspontaneous meaning bond breaking or weakening.[5,9-12]

3. Anisotropy of the induced current density (ACID)

The analysis of the anisotropy of induced current density (ACID), i.e., a function of the paramagnetic part of the current density arising from the response of the wavefunction subject to magnetic field perturbations- is a powerful tool intended to probe, to quantify, and to visualize *delocalized electrons* and *conjugated bonding* in any molecular system.[13,14] The analysis of the isosurfaces of the (non normalized) ACID scalar field provides a visually appealing representation for the anisotropies of the density of only delocalised electrons, i. e., those associated only to the "interatomic currents" or delocalized electrons. Further, the anisotropies associated to either diatropic or paratropic currents are identified by plotting the current density vectors onto the ACID isosurface. Delocalization effects are quantified in terms of the critical isosurface values (CIVs) between two groups or atoms. Higher CIVs reveals stronger delocalisation or conjugation between the associated regions.[13,14]

Following on going interest associated to the study of electron delocalization along reaction processes,[15] in order to study the nature of delocalization in the aryl-aryl di-π-methane rearrangement, the singlet and triplet states of benzene has been chosen as suitable references for comparison (see **Scheme S1**). In the case of benzene (D_{6h}), current vectors onto the ACID 0.05 isosurface evidence that outer ring anisotropies are due to diatropic currents (a clockwise density flow), whereas the inner ring ones can be associated to paratropic currents (a counterclockwise density flow). In the case of triplet benzene (D_{2h}), only paratropic currents are observed.

a) C_6H_6 (s), D_{6h} **b) C_6H_6 (t), D_{2h}**

Scheme S1. ACID 0.050 isosurface plots of C_6H_6 in the a) S_0 and b) T_1 states, respectively.

The picture of delocalization in the singlet and triplet states of benzene are identified as aromatic and antiaromatic conjugations, respectively (see **Scheme S2**). Further, the ACID pattern of delocalisation

for the singlet ground state benzene reveals a single critical isosurface value CIV=**0.0898** that splits the ACID envelope into separate atomic regions. In contrast, the triplet state of benzene exhibits two isosurface critical values, namely CIV =**0.1438**, that splits the ACID eveloping over separated allylic fragments, and CIV=**0.1607** that splits towards the atomic regions.

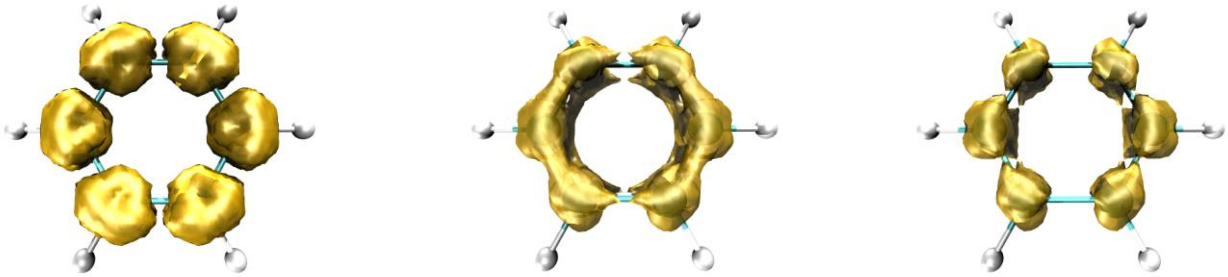

a) C_6H_6 **(s): ACID 0.0898 isosurface** **b)** C_6H_6 **(t): ACID 0.1438 isosurface** **c)** C_6H_6 **(t): ACID 0.1607 isosurface**

Scheme S2. ACID Isosurface plots at the lowest critical isosurface value of C_6H_6 in the a) S_0 and b)-c) T_1 states

The ACID analysis of **DBB*** reveals the existence of four critical isosurface values in the range **0.076-0.082** characterizing the electron delocalization in both rings. The composition of current vectors onto the ACID isosurface around the rings is analogue to the observed one for C_6H_6 (S_0), being therefore identified in terms of aromatic conjugation. The first (lowest) CIV=0.0757 is associated to the simultaneous split of the C1-C2 and C5-C6 ring bonding regions. The remaining ones, in order of increasing value of conjugation, are associated to: (i) the concurrent split C2-C3 and C6-C7 splits (CIV=0.0783), and (ii) the simultaneous split of the C1-C9a, C3-C4, C4-C4a, C5-C10a, C7-C8, and C8-C8a ring bonding regions (CIV=0.082). Such a pattern reveals a symmetrical delocalisation concerning both rings enlighten a lower aromatic character of cyclic conjugation in both rings of **DBB*** as compared to the singlet benzene reference system. Taken the lowest CIV value as a measure of delocalization in each system, it is possible to estimate that each ring of **DBB*** is 16% less aromatic than the singlet benzene system.

The ACID analysis of **TS-I**, **BR-I**, **TS-II**, and **BR-II** reveals the existence of a more asymmetrical situation concerning the delocalization pattern in both rings. The ACID critical isosurface value evidences the participation of one ring (C1-C2-C3-C4-C4a-C9a) in the reaction center, whereas the other (i.e., C5-C6-C7-C8-C8a-C10a) remains essentially unaffected. In any case, along the entire pathway both rings are characterized by a lowest degree of aromatic electron delocalization as compared to benzene (**Table**

S1). Such a decreasing in the degree of conjugation (centered on ring 1) reach a maximum along the **TS-I→BR-I→TS-II** path, which is asscoiated to the bond breaking/bond forming processes centered on the C4a-C9 bonding region. The CIV values (**Table S1**) that the C1-C2-C3-C4-C4a-C9a ring lost electron conjugation as compared to the C5-C6-C7-C8-C8a-C10a one, which exhibits essentially the same pattern of delocalization along the entire series.

Table S1. ACID critical isosurface values (CIV) for selected stationary points along the IRC of the lowest-triplet-state of dibenzobarrelene rearrangement. The bonding region that is separated is indicated following the CIV value.

System	Ring 1 (C1-C2-C3-C4-C4a-C9a)	RPD (Ring 1)	Ring 2 (C5-C6-C7-C8-C8a-C10a)	RPD (Ring 2)
DBB*	**0.0757**: C1-C2 0.0783: C2-C3 0.0810: C4a-C9a 0.0814: C1-C9a 0.0819: C3-C4 0.0819: C4-C4a	-16%	**0.0757**: C5-C6 0.0783: C6-C7 0.0810: C8a-C10a 0.0814: C5-C10a 0.0819: C7-C8 0.0819: C8-C8a	- 16 %
TS-I	**0.0669**: C4a-C9a 0.0734: C2-C3 0.0747: C1-C9a 0.0752: C1-C2 0.0758: C3-C4 0.0769: C4-C4a	-26 %	**0.0795**: C5-C6 0.0827: C6-C7 0.0829: C7-C8 0.0836: C8a-C10a 0.0861: C8-C8a 0.0887: C5-C10a	-11 %
BR-I	**0.0604**: C1-C9a 0.0618: C4-C4a 0.0676: C2-C3 0.0710: C3-C4 0.0725: C1-C2 0.0733: C4-C4a	-33 %	**0.0798**: C5-C6 0.0799: C5-C10a 0.0847: C7-C8 0.0851: C6-C7 0.0860: C8-C8a 0.0860: C5-C10a	-11 %
TS-II	**0.0641**: C1-C9a 0.0689: C2-C3 0.0697: C4a-C9a 0.0716: C1-C2 0.0742: C3-C4 0.0746: C4-C4a	-29 %	**0.0800**: C5-C6 0.0816: C7-C8 0.0821: C5-C10a 0.0829: C6-C7 0.0831: C8a-C10a 0.0868: C8-C8a	-11 %
BR-II	**0.0780**: C1-C2 0.0798: C4-C4a 0.0817: C3-C4 0.0840: C2-C3 0.0878: C1-C9a 0.0890: C4a-C9a	-13 %	**0.0761**: C5-C6 0.0775: C6-C7 0.0784: C8-C8a 0.0793: C5-C10a 0.0805: C8-C10a 0.0881: C7-C8	- 15 %

RPD = Relative percent of delocalization with respect to C_6H_6(s). RPD = [Min CIV(Ring) – Min CIV(C6H6(s))/ Min CIV(C6H6(s)]x100

In all cases, the anisotropies of the induced currents are similar to those observed in singlet benzene (i.e., aromatic conjugation) as evidenced by the current vectors plotted onto the ACID isosurfaces (**Figure S1**).

DBB*

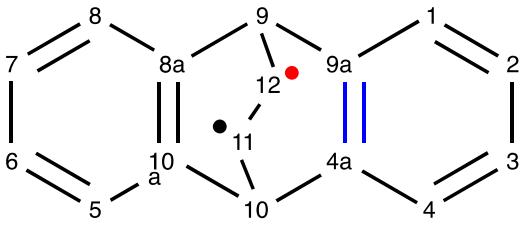

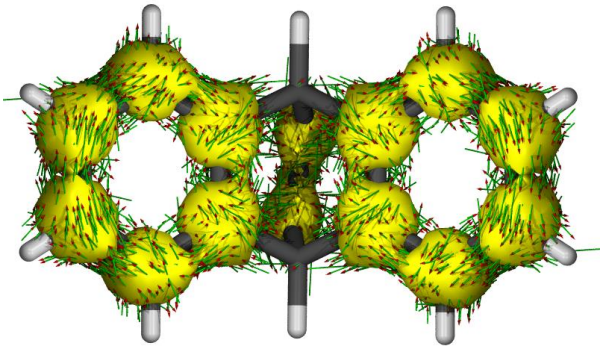

TS-I

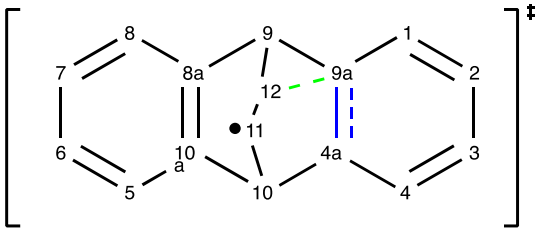

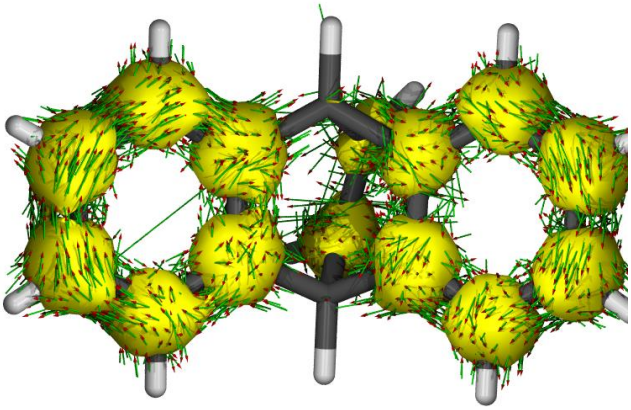

BR-I

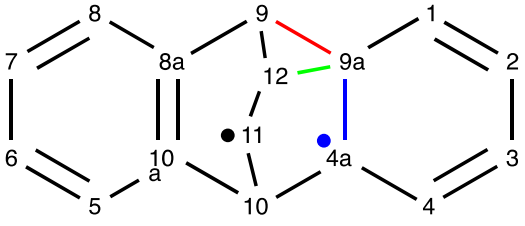

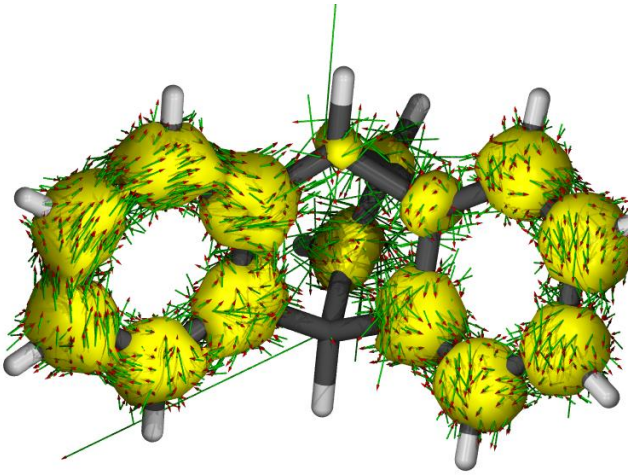

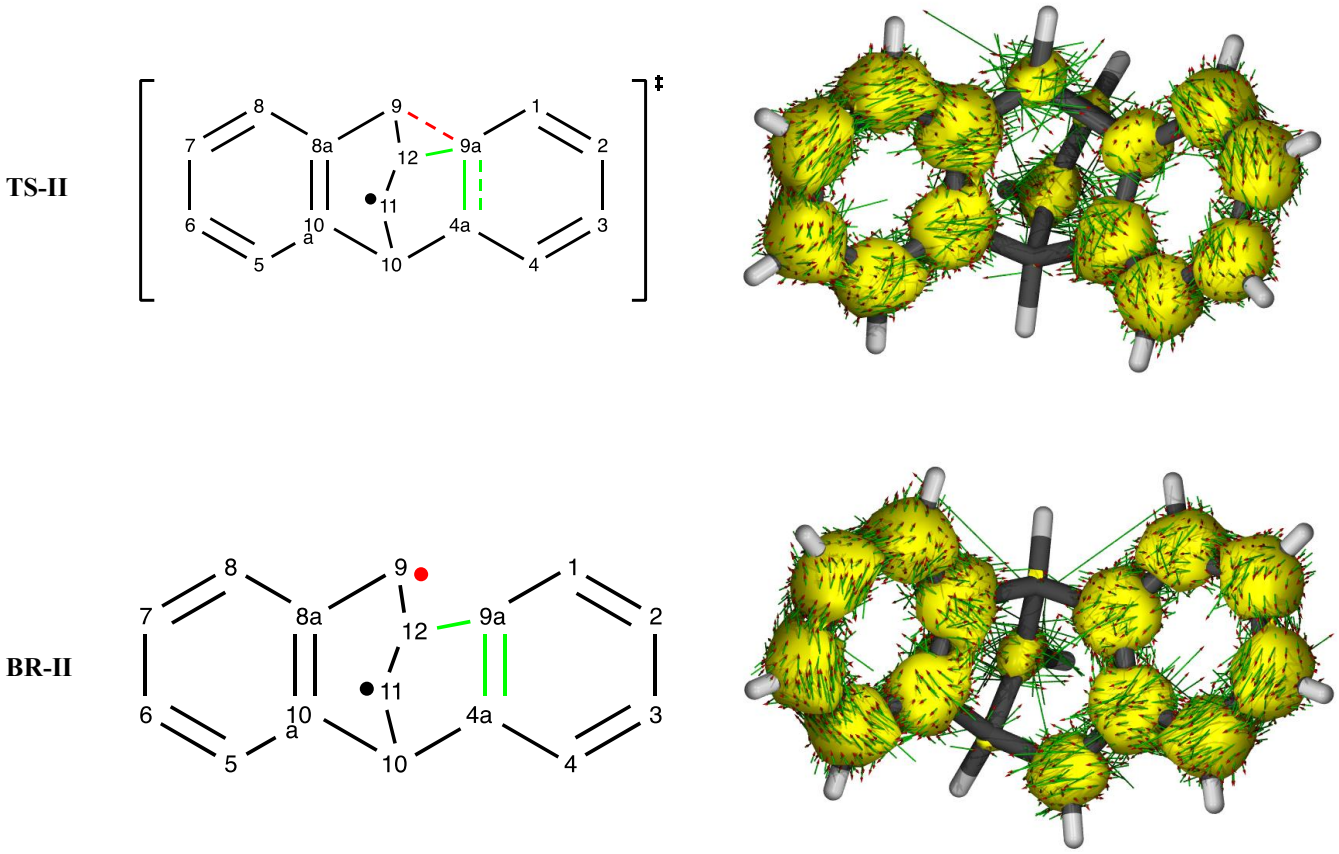

Figure S1. ACID 0.050 isosurface plots of **DBB*, TS-I**, **BR-I**, **TS-II**, and **BR-II** in T_1 state. The vectors plotted onto the ACID isosurface indicate the magnetically induced diatropic (clockwise) and paratropic (anticlockwise) ring currents. The magnetic field vector is parallel to the z-axis pointing out of page (x-y plane), and the observed pattern in either direction will depend on the relative directions of the current flow and the applied magnetic field. In all cases, a lowering of the (aromatic) electron delocalization is revealed for both rings. The center of the reaction is outlined.

4. Topological analysis of electron localisation function (ELF)

An attractive procedure that provides a more straightforward connection between the electron density distribution and the chemical structure is the quantum chemical analysis of the electron localisation function (ELF).[16] ELF is a useful relative measure of the electron pair localisation characterising the corresponding electron-density.[17,18] Within the framework of density functional theory (DFT), [19,20] ELF is a density-based property that can be interpreted in terms of the positive-definite local Pauli and Thomas Fermi kinetic energy densities in a given system. In the validity of such framework, these quantities provide key information to evaluate the relative local excess of kinetic energy density associated to the Pauli principle. ELF becomes valued in the range [0,1], being the highest values

associated with the spatial positions with higher relative electron localisation.[21-23] After an analysis of the electron-density, ELF provides basins of attractors, which are the domains in which the probability of finding an electron pair is maximal. The spatial points in which the gradient of ELF has a maximum value are designated as attractors. ELF basins are classified as core basins, C(...), and valence basins, V(...). The latter are characterised by the synaptic order, *i.e.* the number of atomic valence shells in which they participate. Thus, there are monosynaptic, disynaptic, trisynaptic basins and so on.[24] Monosynaptic basins, labelled V(A), correspond to the lone pairs or non-bonding regions, while disynaptic basins, labelled V(A,B), connect the core of two nuclei A and B and, thus, correspond to a bonding region between A and B. This description recovers the Lewis bonding model, providing a very suggestive graphical representation of the molecular system.

Several theoretical studies have shown that the topological analysis of the ELF offers a suitable framework for the study of the changes of electron-density.[25-36] This methodological approach is used as a valuable tool to understand the bonding changes along the reaction path and, consequently, to establish the nature of the electronic rearrangement associated with a given molecular mechanism within a BET perspective.

A view of the ELF in some molecular planes defined for both six-member rings using colour-filled-maps for each stationary point at in the lowest-triplet-state of dibenzobarrelene (**DBB**) and the analysis of the changes in the number and type of ELF valence basins for some structures involved along the IRC of **DBB*** permit to characterise the corresponding molecular mechanism.

4a. ELF topological analysis in dibenzobarrelene rearrangement

In order to characterise the lowest-triplet-state of dibenzobarrelene rearrangement an ELF topological analysis of the electronic structure of the representative stationary points along the IRC was performed. The populations of the most significant valence basins of the selected structures of the IRC are included in **Table S2**, the attractor positions of the ELF basins for the points involved in this rearrangement are shown in Figure S2 and the colour-filled-maps of the ELF for these stationary points are shown in **Figures S3 and S4**. It is worth to mention that the maps use different colours to represent ELF value in different regions ranging from blue (no electron localization) to red (high electron delocalization).

The topological characteristics at **DBB*** are different from those of the **DBB (S_0)** (see **Table S2 and Figure S2**). Two V(C11) and V(C12) monosynaptic basins related to the two C11 and C12 radical

centers, demanded for the following rearrangements, are present at **DBB*** with electron populations of 0.76e each one as result of the sensitization of the singlet ground state of **DBB**. At **DBB (S_o)** it may be seen two disynaptic basins, V(C11,C12) and V'(C11,C12), integrating a total population of 3.58e, which are associated with the C11−C12 double bonds of the ethylene fragment within the whole structure. The topological characteristics and the electron populations for **DBB*** at both six-member rings are very similar. Note that all disynaptic basins at both rings (for comparisons see **Table S2**) integrate electron population in the range of 2.70e to 2.96e, associated to the delocalized double and single bonds and showing high symmetry in the electron rearrangement in both rings at **DBB***. This electronic pattern is also rather similar to that showed in **DBB (S_o)**. Note that the colour-filled-maps of the ELF for both rings defined by C7-C5-C8a and C2-C4-C9a centers (see **Figure S3**) are qualitatively comparable each other revealing that the rings present the same delocalization topology pattern and high similitude to that showed by benzene (S_o), which is used as reference of the most delocalized system.

At **TS-I**, the most noticeable topological change is a strong decrease of the electron population of the V(C12) monosynaptic basin to 0.31e, while the population of the V(C11) monosynaptic basin has slightly decreased to 0.70e. In comparison with similar C-C bonds found in **DBB*** (see **Table S2 and Figure S2**) note that the decrease of population of the V(C12) monosynaptic basin can be seen as a delocalization towards the C9-C12 single bond and in consequence an increase in the population of V(C9,C12) disynaptic basin by *c.a.* 0.22e is observed. Also note a slight increase in the electron populations of the V(C11,C12) disynaptic basin to 2.15e. It is worth to mention other relevant topological change in one of the rings at **TS-I**. The electron population at V(C1,C2) and V(C4,C4a) disynaptic basins increase to 3.08e and 3.16e, respectively, when they are compared with the corresponding analogue ring where the electron population is maintained in the range of 2.71e to 2.94e. The corresponding colour-filled-maps of the ELF for **TS-I** in the plane defined by C7-C5-C8a and C2-C4-C9a centers (see **Figure S4a and S4b**) qualitatively are not so evident showing that topological electronic change.

At **BR-I**, relevant topological changes have occurred. Only one V(C11) monosynaptic basin with a electron population of 0.62e remains, while a new V(C9a,C12) disynaptic basin is formed integrating a population of 1.69e. Note that a cyclopropane between C12, C9 y C9a centers is formed as a result of this new electron rearrangement (see **Table S2 and Figure S2**). Interestingly, one of the six-member rings (right-side) shows a different redistribution of populations compared with the corresponding left-side ring. The electron population of V(C4a,C9a) disynaptic basin is 2.16e; the corresponding for V(C1,C9a) disynaptic basin is 2.19e; a increase for V(C1,C2) disynaptic basin is observed, 3.28e;

the populations of V(C2,C3) and V(C3,C4) disynaptic basins slightly decrease to 2.67e and 2.58e, compared with that shown in **TS-I** and finally for V(C4,C4a) disynaptic basin is increased to 3.34e. Note that there is a strong accumulation of electron population associated with C1-C2 and C4-C4a bonds. Probably the increase of population on these disynaptic basins is a consequence of the delocalization of the radical species shown in **Figure S2** on the six-member ring. The second left-side six-member ring shows electron populations in the range 2.69e – 2.95e for the dysinaptic basins. The colour-filled-maps of the ELF for **BR-I** in the plane defined by C2-C4-C9a atoms qualitatively show a difference in the contour lines compared with the map symmetrically located and defined by C7-C5-C8a atoms as shown in **Figure S4c and S4d**. This change indicates an electronic picture completely different of the six-member rings at **BR-I**.

At **TS-II**, a new relevant topological change has occurred: cyclopropane formed at **BR-I** is not present at **TS-II** and concomitantly one V(C9) monosynaptic basin integrating 0.87e is created (see **Table S4 and Figure S2**). While the V(C11) monosynaptic basin increases slightly its population to 0.66e, the right-side six member ring the population of V(C4a,C9a) disynaptic basin increases by 0.20e; the same pattern is observed for the V(C1,C9a) disynaptic basin reaching a population of 2.41e; slight decrease for V(C1,C2) and V(C4,C4a) disynaptic basins by *c.a.* 0.15e and 0.11e and finally, the populations of V(C2,C3) and V(C3,C4) disynaptic basins slightly increase to 2.76e and 2.64e, compared with that shown in **BR-I**. Note that the populations of the left-side ring are in the range 2.65e – 2.87e. In summary, the electronic rearrangement is mainly observed on the right-side ring, even though at **TS-II**, the small difference observed in the electronic distribution on both six-member rings is not completely sensed by the colour-filled-maps of the ELF in the planes defined by C7-C5-C8a and C2-C4-C9a centers (see **Figure S4e and S4f**).

Finally, at **BR-II**, a relevant change along the reaction path takes place at this last point: the V(C9) monosynaptic basin created at **TS-II** has disappeared, the V(C11) monosynaptic basin remains integrating 0.71e, while the population of V(C8a,C9) disynaptic basin is increased by ca. 0.63e (see **Table S2 and Figure S2**). Note that the populations of right-side six-member ring are ranging 2.71e – 2.96e, while those of the left-side ring are tween 2.57e- 3.00e. These results are in good agreement with the population of bot rings in **DBB** (S_0). It may be seen that the at this point the delocalization of single and double bond is recovered. The colour-filled-maps of the ELF in the planes defined by C7-C5-C8a and C2-C4-C9a centers at **BR-II** support this result (see **Figures S4g and S4h**).

Table S2. Valence basin populations N calculated from the ELF of the selected stationary points along the IRC of the lowest-triplet-state of dibenzobarrelene rearrangement. Electron populations are given in e.

	DBB (S_0)	**DBB***	**TS-I**	**BR-I**	**TS-II**	**BR-II**
V(C11,C12)	1.79	2.10	2.15	2.12	2.06	1.97
V'(C11,C12)	1.79					
V(C11)		0.76	0.70	0.62	0.66	0.71
V(C12)		0.76	0.31			
V(C9,C12)	1.93	1.89	2.11	1.76	1.93	1.99
V(C10,C11)	1.93	1.89	1.92	1.96	1.97	1.96
V(C8a,C9)	1.93	2.00	2.04	2.12	2.28	2.91
V(C10,10a)	1.97	1.94	1.97	1.95	1.94	1.96
V(C9a,C9)	1.97	1.94	1.96	1.63		
V(C4a,C10)	1.92	1.99	1.99	1.98	1.97	1.96
V(C9a,C12)				1.69	1.88	1.93
V(C9)					0.87	
V(C4a,C9a)	2.67	2.70	2.63	2.16	2.36	2.71
V(C1,C9a)	3.00	2.94	2.54	2.19	2.41	2.95
V(C1,C2)	2.70	2.74	3.08	3.28	3.13	2.73
V(C2,C3)	2.93	2.88	2.76	2.67	2.76	2.88
V(C3,C4)	2.70	2.73	2.69	2.58	2.64	2.72
V(C4,4a)	3.00	2.96	3.16	3.34	3.23	2.96
V(C8a,10a)	2.67	2.70	2.71	2.69	2.65	2.57
V(C8,C8a)	3.00	2.96	2.94	2.90	2.82	2.61
V(C7,C8)	2.70	2.73	2.74	2.77	2.87	2.99
V(C6,C7)	2.93	2.87	2.85	2.85	2.82	2.74
V(C5,C6)	2.70	2.74	2.75	2.75	2.75	2.73
V(C5,C10a)	3.00	2.94	2.93	2.95	2.75	3.00

Figure S2. ELF attractor positions for selected points along the IRC of the lowest-triplet-state of dibenzobarrelene. The electron populations are given in electron units (e).

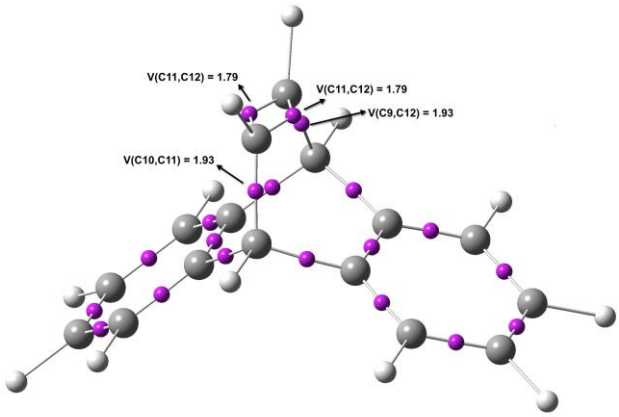

DBB (S_0)

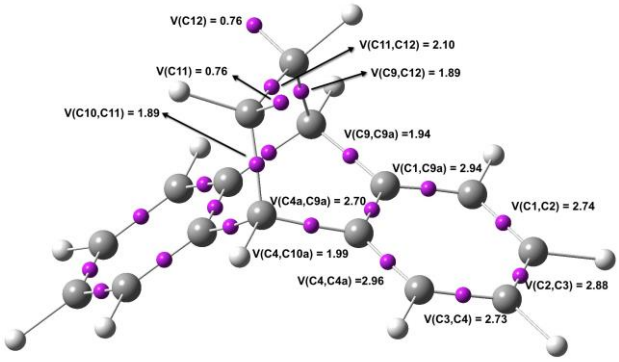

DBB*

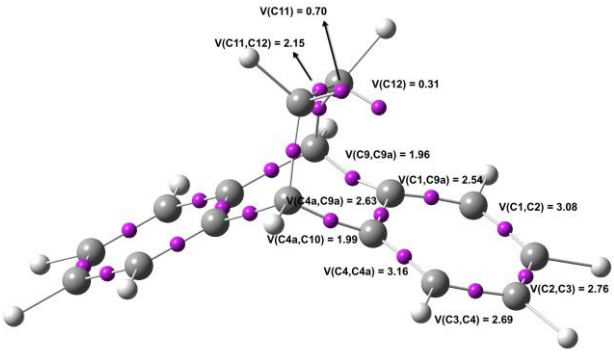

TS-I

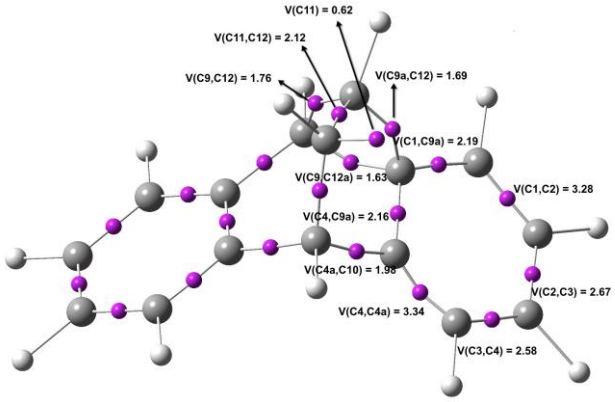

BR-I

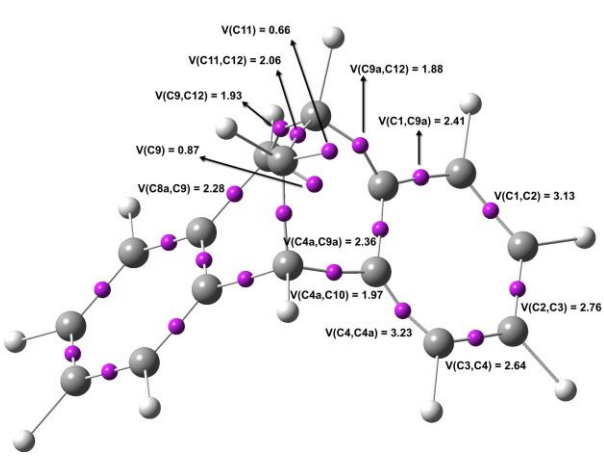

TS-II

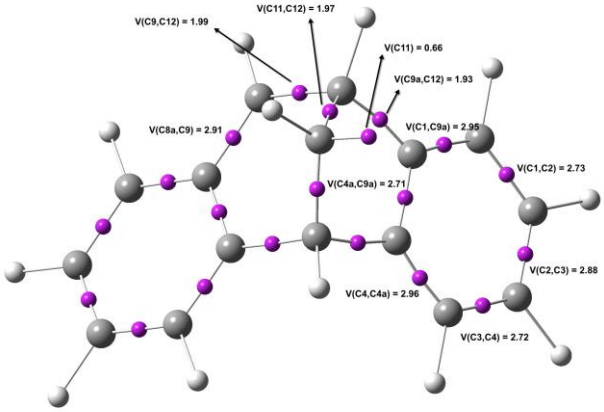

BR-II

Figure S3. Colour-filled maps of the electron localization function (ELF), in two molecular planes of **DBB*** defined by the (a) C7-C5-C8a centers, (b) C2-C4-C9a centers, and (c) benzene (S_o) at (U)M062x/6-31G(d) level.

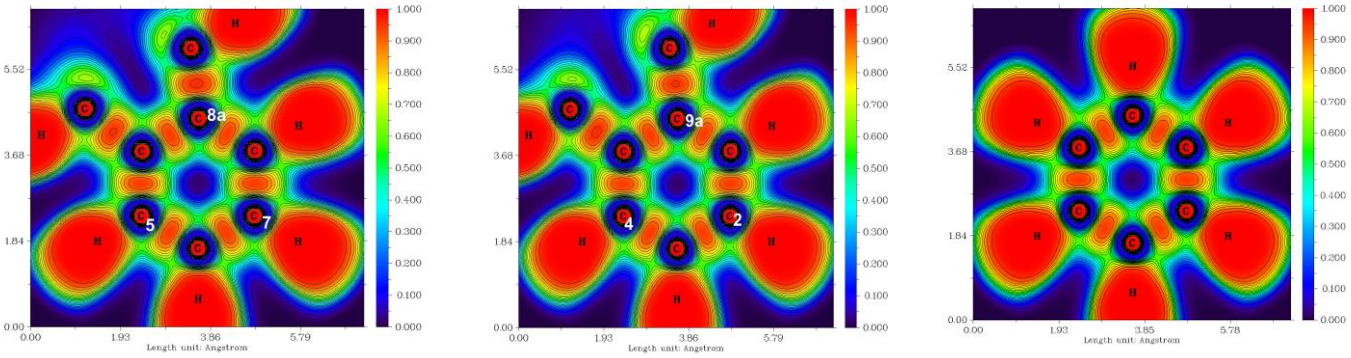

(a) **(b)** **(c) Benzene**

Figure S4. Colour-filled maps of the electron localization function (ELF), in two molecular planes defined by the (a) C7-C5-C8a and (b) C2-C4-C9a centers of **TS-I**; (c) C7-C5-C8a and (d) C2-C4-C9a centers of **BR-I**; (e) C7-C5-C8a and (f) C2-C4-C9a centers of **TS-II** and (f) C7-C5-C8a and (h) C2-C4-C9a centers of **BR-II** obtained at (U)M062x/6-31G(d) level.

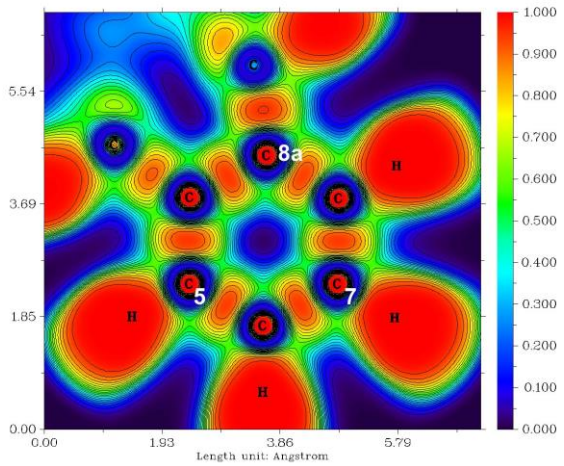

(a)

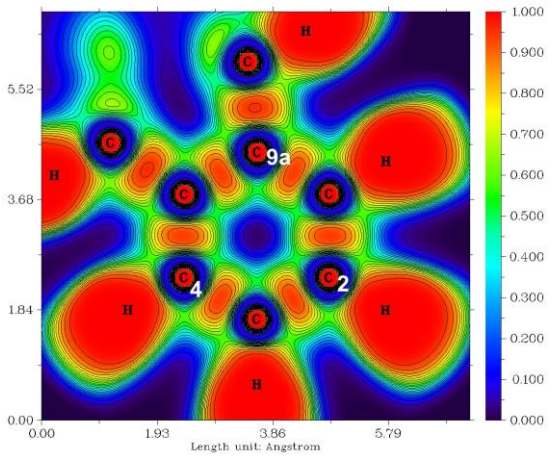

(b)

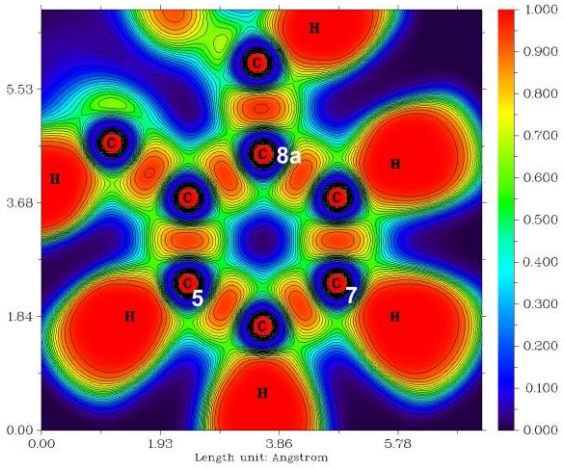

(c)

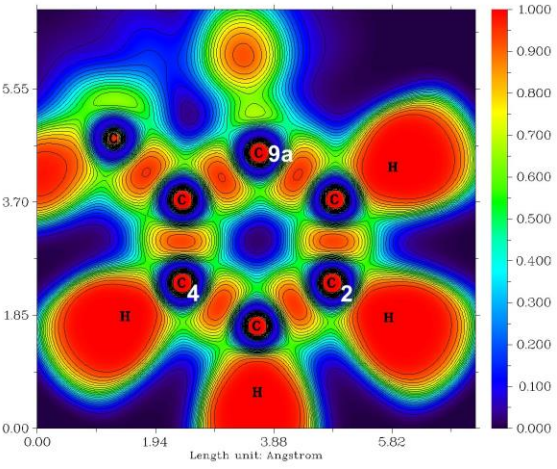

(d)

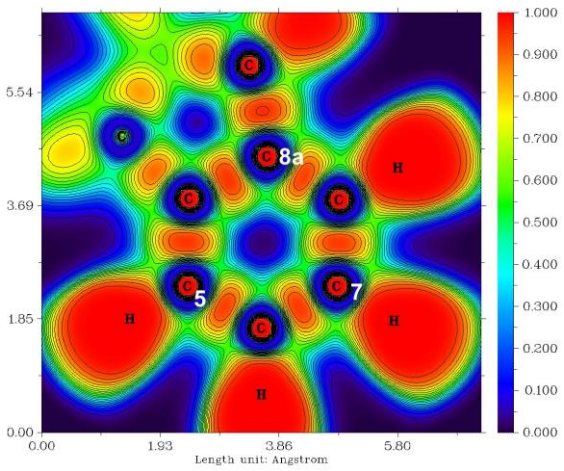
C
8a
H
5
7
0.00
1.93
3.86
5.80
5.54
3.69
1.85
0.00
Length unit: Angstrom
1.000
0.900
0.800
0.700
0.600
0.500
0.400
0.300
0.200
0.100
0.000

(e)

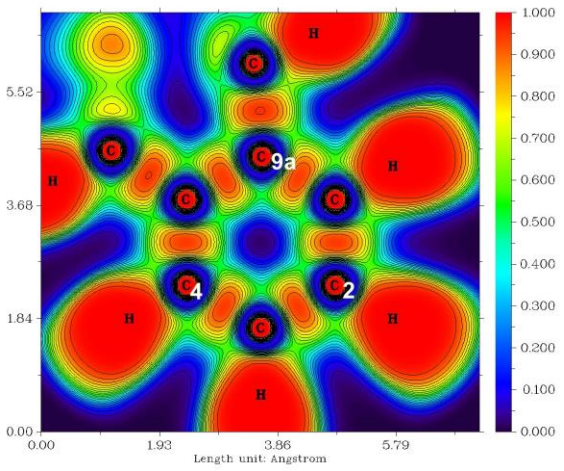
H
C
9a
4
2
0.00
1.93
3.86
5.79
5.52
3.68
1.84
0.00
Length unit: Angstrom
1.000
0.900
0.800
0.700
0.600
0.500
0.400
0.300
0.200
0.100
0.000

(f)

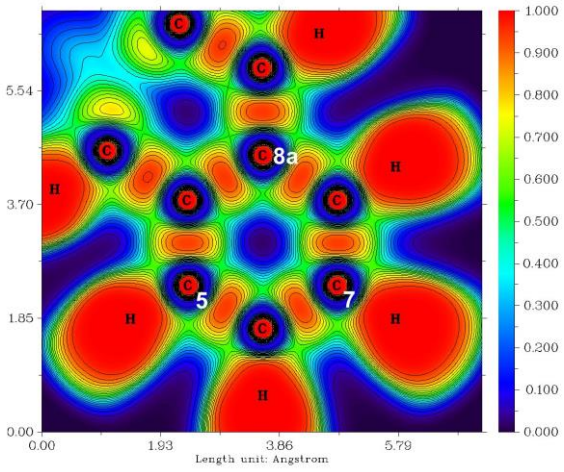
C
H
8a
5
7
0.00
1.93
3.86
5.79
5.54
3.70
1.85
0.00
Length unit: Angstrom
1.000
0.900
0.800
0.700
0.600
0.500
0.400
0.300
0.200
0.100
0.000

(g)

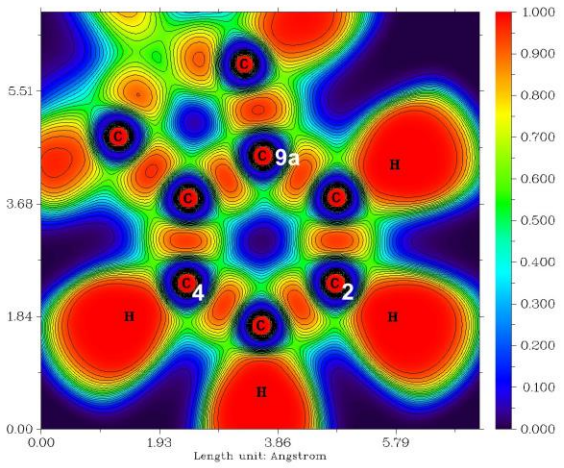
C
9a
4
2
H
0.00
1.93
3.86
5.79
5.51
3.68
1.84
0.00
Length unit: Angstrom
1.000
0.900
0.800
0.700
0.600
0.500
0.400
0.300
0.200
0.100
0.000

(h)

5. Additional Computational Details

The topological analysis of ELF was performed with the Topmod [37] programs and the Multiwfn[38] suite of tools by using the UM06-2X/6-31G(d) level of theory of the relevant structures along the lowest-triplet-state of **DBB**. A view of the ELF in some molecular planes defined for both six-member rings using colour-filled-maps for each stationary point at in the lowest-triplet-state of dibenzobarrelene (**DBB**) and the analysis of the changes in the number and type of ELF valence basins for some structures involved along the IRC of **DBB*** permit to characterise the corresponding molecular mechanism.

6. References

(1) Toro-Labbe, A.; Gutierrez-Oliva, S.; Concha, M. C.; Murray, J. S.; Politzer, P. *J. Chem. Phys.* 2004, *121*, 4570.
(2) Toro-Labbé, A. *J. Phys. Chem. A* 1999, *103*, 4398.
(3) Politzer, P.; Reimers, J. R.; Murray, J. S.; Toro-Labbé, A. *J. Phys. Chem. Lett.* 2010, *1*, 2858.
(4) Herrera, B.; Toro-Labbé, A. *J. Chem. Phys.* 2004, *121*, 7096.
(5) Herrera, B.; Toro-Labbe, A. *J Phys Chem A* 2007, *111*, 5921.
(6) Gutierrez-Oliva, S.; Herrera, B.; Toro-Labbe, A.; Chermette, H. *J Phys Chem A* 2005, *109*, 1748.
(7) Geerlings, P.; De Proft, F.; Langenaeker, W. *Chem Rev* 2003, *103*, 1793.
(8) Parr, R. G.; Yang, W. *Density Functional Theory of Atoms and Molecules 1989, New York, Oxford University Press*.
(9) Zimmerman, H. E.; Grunewald, G. L. *J. Am. Chem. Soc.* 1966, *88*, 183
(10) Toro-Labbe, A.; Gutierrez-Oliva, S.; Murray, J. S.; Politzer, P. *J Mol Model* 2009, *15*, 707.
(11) Echegaray, E.; Toro-Labbe, A. *J. Phys. Chem. A* 2008, *112*, 11801.
(12) Cerón, M. L.; Echegaray, E.; Gutierrez-Oliva, S.; Herrera, B. *Sci. China Chem.* 2011, *54*, 1982.
(13) Geuenich, D.; Hess, K.; Kohler, F.; Herges, R. *Chemical Reviews* 2005, *105*, 3758.
(14) Herges, R.; Geuenich, D. *Journal of Physical Chemistry A* 2001, *105*, 3214.
(15) Domingo, L. R.; Rios-Gutierrez, M.; Chamorro, E.; Perez, P. *Chemistryselect* 2016, *1*, 6026.
(16) Becke, A. D.; Edgecombe, K. E. *Journal of Chemical Physics* 1990, *92*, 5397.
(17) Savin, A.; Silvi, B.; Colonna, F. *Can. J. Chem.* 1996, *74*, 1088.
(18) Silvi, B.; Savin, A. *Nature* 1994, *371*, 683.
(19) Geerlings, P.; De Proft, F.; Langenaeker, W. *Chem. Rev.* 2003, *103*, 1793.
(20) Parr, R. G.; Yang, W. *J. Am. Chem. Soc.* 1984, *106*, 4049.
(21) Savin, A.; Becke, A. D.; Flad, J.; Nesper, R.; Preuss, H.; Vonschnering , H. G. *Angew. Chem. Int. Ed.* 1991, *30*, 409.
(22) Savin, A.; Nesper, R.; Wengert, S.; Fassler, T. F. *Angew. Chem., Int. Ed. Engl.* 1997, *36*, 1809.
(23) Savin, A. *Journal of Chemical Sciences* 2005, *117*, 473.
(24) Thom, R. *Structural Stability and Morphogenesis: An Outline of a General Theory of Models*; Inc.:Reading, MA, 1976.
(25) Andrés, J.; González-Navarrete, P.; Safont, V. *Int. J. Quantum Chem.* 2014, *114*, 1239.
(26) Berski, S.; Andres, J.; Silvi, B.; Domingo, L. R. *J. Phys. Chem. A* 2006, *110*, 13939.
(27) Berski, S.; Andrés, J.; Silvi, B.; Domingo, L. R. *J. Phys. Chem. A* 2003, *107*, 6014.
(28) Polo, V.; Andrés, J.; Berski, S.; Domingo, L. R.; Silvi, B. *J. Phys. Chem. A* 2008, *112*, 7128.
(29) Domingo, L. R.; Chamorro, E.; Pérez, P. *J. Org. Chem.* 2008, *73*, 4615
(30) Domingo, L. R.; Chamorro, E.; Pérez, P. *Org. Biomol. Chem.* 2010, *8*, 5495.
(31) Domingo, L. R.; Ríos-Gutiérrez, M.; Duque-Noreña, M.; Chamorro, E.; Pérez, P. *Theor. Chem. Acc.* 2016, *135*, 160.
(32) Domingo, L. R.; Ríos-Gutiérrez, M.; Sáez, J. A. *RSC Adv.* 2015, *5*, 37119.
(33) Domingo, L. R.; Ríos-Gutiérrez, M.; Pérez, P. *Tetrahedron* 2016, *72*, 1524.
(34) Chamorro, E.; Santos, J. C.; Gomez, B.; Contreras, R.; Fuentealba, P. *Journal of Physical Chemistry A* 2002, *106*, 11533.
(35) Matito, E.; Poater, J.; Bickelhaupt, F. M.; Sola, M. *Journal of Physical Chemistry B* 2006, *110*, 7189.

(36) Matito, E.; Silvi, B.; Duran, M.; Sola, M. *Journal of Chemical Physics* **2006**, *125*.
(37) Noury, S.; Krokidis, X.; Fuster, F.; Silvi, B. *Comput. Chem.* **1999**, *23*, 597.
(38) Lu, T.; Chen, F. W. *Journal of Computational Chemistry* **2012**, *33*, 580.

7. Cartesian coordinates of optimized geometries

DBB* (M06-2x/6-31G(d))

C	0.01043300	0.15575900	0.00285300
C	0.03307800	0.12023200	1.39867700
C	1.24657700	-0.01888700	2.05762800
C	2.44423600	-0.10074600	1.32802700
C	2.41839300	-0.06100500	-0.05762900
C	1.19525400	0.06437500	-0.72092500
C	1.45931800	-0.03431400	3.56851200
C	3.67985300	-0.23078600	2.19824100
C	3.44453600	-1.40092400	3.14888500
C	2.26275200	-1.27838400	3.89816200
C	1.93017400	-2.24482300	4.83490000
H	1.01419200	-2.15068100	5.41271200
C	2.77963600	-3.33672200	5.02956800
C	3.95513900	-3.45203200	4.29407000
C	4.29510000	-2.47846300	3.35264300
H	-0.93693800	0.25424100	-0.51841300
H	-0.89094600	0.19280900	1.96667100
H	3.34541300	-0.12678500	-0.62151600
H	1.17072700	0.09146800	-1.80598700
H	2.52084300	-4.09759400	5.75968500
H	4.61136700	-4.30262900	4.45181500
H	5.21383100	-2.56406200	2.77790600
H	0.51668800	0.02578300	4.11940900
H	4.60119100	-0.34584300	1.62067300
C	3.71023200	0.94089200	3.17783800
C	2.35856100	1.18601000	3.75314900
H	1.87695000	2.14639800	3.57031100
H	4.57418200	0.96125300	3.84197200

TS-I (M06-2x/6-31G(d))

C	-0.05089800	0.25535200	-0.03907700
C	-0.01257200	0.18317000	1.35405600
C	1.20083800	-0.01205700	2.00011400
C	2.38442900	-0.12881900	1.25462700
C	2.34321200	-0.05889300	-0.13163500
C	1.12167100	0.13382300	-0.77868600
C	1.40504200	-0.09179300	3.50495800
C	3.63003000	-0.34374800	2.06403400
C	3.44601800	-1.35241500	3.17722700
C	2.16696800	-1.35825900	3.82311600
C	1.85979600	-2.32115800	4.75838400
H	0.89894000	-2.29147800	5.26590400
C	2.79408900	-3.31924700	5.07002600
C	4.05339700	-3.31577500	4.45503400
C	4.39167400	-2.35325100	3.52125900
H	-0.99918300	0.40617600	-0.54583400
H	-0.92688600	0.27562900	1.93499800
H	3.26069300	-0.15320300	-0.70709400
H	1.08820100	0.18912400	-1.86240300
H	2.54737000	-4.08599600	5.79672600
H	4.77140900	-4.09231700	4.70282900
H	5.35992000	-2.37188100	3.02839900
H	0.46661000	0.01218200	4.05612900
H	4.54287900	-0.48789300	1.48529800
C	3.74927800	0.52972000	3.28213600
C	2.44633100	0.97427300	3.82442900
H	2.15007700	2.02109900	3.79254000
H	4.71367700	0.74038100	3.72423300

BR-I (M06-2x/6-31G(d))

C	-0.15318800	0.39755800	0.17851600
C	0.01069600	0.12302100	1.50865300
C	1.35532900	-0.09994600	2.03299500
C	2.47963800	0.09656700	1.09989800
C	2.27216500	0.39146900	-0.21233300
C	0.94955900	0.52117200	-0.70131000
C	1.64064200	-1.20259200	3.09653700
C	3.74997600	-0.01697700	1.91542900
C	3.92559700	-1.49431400	2.24609300
C	2.80542300	-2.08657900	2.85485500
C	2.83808500	-3.43733000	3.18748600
H	1.97122300	-3.89968200	3.65275400
C	3.98193600	-4.19163600	2.92797400
C	5.09267600	-3.59944200	2.33369200
C	5.06322800	-2.24715100	1.99079800
H	-1.15579500	0.53458600	-0.21655300
H	-0.84109400	0.04051600	2.17819600
H	3.11592500	0.55219500	-0.87863200
H	0.77963500	0.74529600	-1.74825800
H	4.00371000	-5.24459600	3.19176500
H	5.98182300	-4.18902400	2.13223800
H	5.92480300	-1.77974200	1.52036000
H	0.75193600	-1.64626700	3.53784900
H	4.63864100	0.40895100	1.44273000
C	3.31054700	0.66060400	3.20055700
C	1.90377300	0.26153600	3.41990500
H	1.27460500	0.74503400	4.15919400
H	3.99987100	0.88994700	4.00498200

TS-II (M06-2x/6-31G(d))

C	0.00640500	0.01424500	0.01776400
C	0.00487900	-0.00270200	1.41341100
C	1.20412000	-0.00144500	2.10981000
C	2.43296300	0.03027500	1.41401800
C	2.42282100	0.01827500	0.01611500
C	1.21523500	0.01767000	-0.67546900
C	1.33573800	-0.09136200	3.62701400
C	3.65630500	0.03876000	2.20543200
C	3.55253900	-0.97299700	3.68545400
C	2.17224300	-1.32989300	3.89481800
C	1.81541400	-2.62113000	4.18467700
H	0.77056200	-2.88496400	4.32652200
C	2.81855900	-3.60031300	4.31858000
C	4.17264700	-3.25606300	4.16902500
C	4.56174000	-1.96345400	3.87895900
H	-0.93329600	0.01616000	-0.52567400
H	-0.93406200	-0.02704700	1.96139500
H	3.36457600	0.02531200	-0.52673900
H	1.21775000	0.02136100	-1.76116000
H	2.54625800	-4.62298500	4.55613600
H	4.93185600	-4.02077500	4.30430700
H	5.61183000	-1.69866600	3.79279400
H	0.36067300	-0.07621800	4.12136200
H	4.61662900	-0.07693200	1.71242700
C	3.64360400	0.53257800	3.62608700
C	2.29505700	1.00598100	4.04198900
H	4.53827300	1.03363400	3.98713800
H	2.01261600	2.05270100	4.03662400

BR-II (M06-2x/6-31G(d))

C	0.08253200	-0.32742900	0.08472600
C	0.07753600	-0.16866300	1.47411400
C	1.28547800	0.03559500	2.12020400
C	2.48777100	0.06419600	1.40321200
C	2.49747500	-0.11459500	0.03022300
C	1.27828000	-0.30229600	-0.62868400
C	1.93063200	-1.20984700	4.12664100
C	3.63866100	0.25416900	2.38493900

C	4.07090500	-1.11708000	2.90131200
C	3.15629800	-1.81787100	3.74892100
C	3.51986800	-3.11057500	4.19318400
H	2.82931700	-3.65700300	4.83074000
C	4.73410900	-3.67246800	3.83863200
C	5.62496200	-2.96761100	3.02504700
C	5.28336900	-1.69494700	2.56261700
H	-0.85575400	-0.47128300	-0.44245000
H	-0.85589900	-0.19607700	2.02981900
H	3.43013600	-0.10232000	-0.52750200
H	1.26382800	-0.42824600	-1.70703000
H	4.99520900	-4.66385200	4.19619900
H	6.57787000	-3.40796400	2.74897700
H	5.97056800	-1.14670700	1.92221600
H	1.20066800	-1.76584100	4.70646900
H	4.49220200	0.80100900	1.97304400
C	2.91648800	0.93205900	3.52430700
C	1.60883400	0.17980200	3.60916100
H	0.82318400	0.66246300	4.19609400
H	3.43416400	1.29287600	4.40727800